Finite Temperature Properties of $(CO_2)_n$ Clusters

Hanbin Liu and Kenneth D. Jordan*

Department of Chemistry and Center for Molecular and Materials Simulations, University of Pittsburgh, Pittsburgh, Pennsylvania 15260

Received: March 2, 2003; In Final Form: May 26, 2003

The parallel-tempering Monte Carlo procedure is used to characterize the $(CO_2)_n$, $n = 6$, 8, 13, and 19, clusters. The heat capacity curves of the $n = 13$ and 19 clusters are found to have pronounced peaks that can be associated with cluster melting. In addition, there is evidence of a low temperature "solid ↔ solid" transition in the case of $(CO_2)_{19}$. The low-energy minima and rearrangement pathways are determined and used to examine the complexity of the potential energy surfaces of the clusters.

1. Introduction

Carbon dioxide has attracted considerable experimental and theoretical attention both because of the importance of its supercritical state for chemical separations and because it is a prototype for molecules for which the dominant electrostatic interactions are quadrupole−quadrupole in nature.[1] Despite this, our knowledge of the properties of CO_2 clusters lags behind that for clusters of polar molecules such as water. Although several Monte Carlo and molecular dynamic simulations of $(CO_2)_n$ clusters have been carried out, [2−6] there remain unresolved issues including the connections between the thermodynamic behavior and the topology of the underlying potential energy surfaces. Also, it appears that some of the earlier simulations failed to achieve equilibrium, particularly at the lowest temperatures considered.

In the present study the parallel-tempering Monte Carlo method,[7] which is well suited for achieving equilibrium in low-temperature simulations when there are large energy barriers separating low-lying local potential energy minima, is combined with long production cycles to calculate the finite-temperature behavior of the $(CO_2)_n$, $n = 6$, 8, 13, and 19, clusters. To aid in analyzing the nature of the transitions associated with peaks in the heat capacity curves, the populations of inherent structures are calculated as a function of temperature. For each cluster considered, the low-energy minima and transition states are located using the eigenmode-following method[8−10] and used to construct disconnectivity graphs to provide insight into the topology of the potential energy surface, in particular, the accessibility of different regions of configuration space as a function of energy.

2. Methodology

2.a. Model Potential. The $CO_2−CO_2$ interactions are described by a two-body model potential due to Murthy et al.[11] This is a rigid monomer model with CO bond lengths equal to the experimental (R_e) value and interactions between monomers described by electrostatic and 6−12 Lennard-Jones terms. The former are incorporated by means of five point charges on each monomer, the locations and values of which are given in Table 1. The Lennard-Jones terms are atom−atom in nature, with the parameters being given in Table 2.

TABLE 1: Location of the Point Charges in the Murthy CO_2 Potential[a]

site	Z(Å)	Q(e)
1	−1.5232	0.1216
2	−1.0663	−0.6418
3/C[b]	0	1.0404
4	1.0663	−0.6418
5	1.5232	0.1216

[a] Ref 11. [b] The third point charge is located on the C atom.

TABLE 2: Lennard-Jones Parameters for the Murthy CO_2 Model Potential[a]

atom pair	ϵ(K)	σ(Å)
C−C	26.3	2.824
O−O	75.2	3.026
C−O	44.5	2.925

[a] Ref 11.

For $(CO_2)_2$ and $(CO_2)_3$ the Murthy potential gives structures and binding energies in good agreement with the results of experiment and MP2 calculations.[12,13] At first glance, the success of the Murthy potential for describing $(CO_2)_2$ and $(CO_2)_3$ is somewhat surprising since it does not include an explicit induction contribution, which has been shown by symmetry-adapted perturbation theory (SAPT) calculations to be important for these clusters.[14] This suggests that either the LJ or the electrostatic term (or perhaps both) in the Murthy potential is too attractive, thereby "mimicking" the induction interactions. The use of enhanced electrostatic terms to incorporate induction is a common procedure, with a representative example being the TIP4P model for water.[15]

2.b. Parallel Tempering Monte Carlo Procedure. The Monte Carlo simulations were carried out using the parallel tempering algorithm,[16,17] in which simulations over the range of temperatures of interest are carried out in parallel. The sets of configurations generated at the various temperatures are called "replicas". Most moves are "local", i.e., confined to individual replicas, with trial moves translations or rotations of individual molecules, being accepted or rejected according to the Metropolis algorithm:

$$P_{i\to j} = \min\{1, \exp[-\beta(E_j - E_i)]\} \quad (1)$$

where $P_{i\to j}$ is the probability for accepting a move from configuration "i" with energy E_i to configuration "j" with energy

* Author to whom correspondence should be addressed. E-mail: Jordan@psc.edu.

10.1021/jp0345295 CCC: $25.00
Published on Web 07/04/2003

E_j, and b is related to the inverse temperature via $b = (kT)^{-1}$. In the implementation of the parallel tempering algorithm used in the present study, the local moves were carried out by attempting, in succession, translation and rotation of molecules selected at random. The maximum step sizes were chosen so as to maintain close to 50% acceptance ratios. The remaining moves involved attempted swaps of configurations between replicas at adjacent temperature. The acceptance probability for an attempted exchange of configurations from the T_i and T_{i+1} replicas is given by

$$P_{i\rightarrow i+1} = \min\{1, \exp[(\beta_i - \beta_{i+1})(E_i - E_{i+1})]\} \qquad (2)$$

where $b_i = (kT_i)^{-1}$. Exchanges were attempted once every 100 moves, and were made only between replicas at adjacent temperatures. On odd swap cycles, the attempted exchanges were between the (T_1, T_2), (T_3, T_4), etc., replicas, and on even cycles, between the (T_2, T_3), (T_4, T_5), etc., replicas. Additional details on the parallel tempering code used to carry out the simulations are given in ref 18.

At the highest temperatures used in the simulations, evaporative events could occur, which would seriously impact convergence. This problem was avoided in the simulations on the three smaller clusters by rejecting moves that placed one or more of the molecules over a specified distance [6 Å for $(CO_2)_6$ and $(CO_2)_8$, and 8 Å for $(CO_2)_{13}$] from the center of mass of the cluster. For $(CO_2)_{19}$, moves that placed the C atom of an individual monomer more than 5 Å from the C atoms of all other monomers in the cluster were rejected.

One of the challenges in carrying out parallel-tempering Monte Carlo simulations is the choice of an appropriate grid of temperatures. The temperature range should encompass regions over which the structural transformations of interest occur. It is also essential that all important energy barriers are readily overcome at the highest temperature employed and that there is appreciable overlap between the potential energy distributions from the simulations at adjacent temperatures. In the present study, twenty temperatures spanning 20−150 K were used for $(CO_2)_n$, $n = 6$, 8, 13, and twenty-four temperatures spanning 20−200 K were used for $(CO_2)_{19}$. These temperature ranges were chosen on the basis of a series of preliminary parallel-tempering Monte Carlo simulations with different choices of the temperatures. Additional simulations, employing up to thirty-two temperatures, were also carried out, but are not reported here since the results obtained were very close to those from the simulations using fewer temperatures.

For each cluster studied, two parallel-tempering Monte Carlo simulations were carried out, one starting from a configuration chosen at random from a preliminary high-temperature Metropolis Monte Carlo simulation, and the other starting from the global minimum structure. Comparison of the results of the two simulations provides a check on attainment of equilibrium. For each simulation, averaging was done over 2×10^7 moves following an equilibration period, which ranged from 10^7 moves for $(CO_2)_6$ and $(CO_2)_8$ to 2×10^7 moves for $(CO_2)_{13}$ and 3×10^7 moves for $(CO_2)_{19}$. The heat capacity was calculated using

$$C_{N,V,T}(T) = \frac{\langle U^2\rangle - \langle U\rangle^2}{RT^2} \qquad (3)$$

where R is the gas constant.

For monitoring convergence of the simulations and for interpreting structural transformations, it is useful to examine the distributions of inherent structures, obtained by "quenching" configurations sampled in the simulations. In the present study, 500 configurations, chosen at equal intervals, were saved from each replica and optimized to their inherent structures by use of the eigenmode-following method as implemented in the Orient 4.3 program.[19]

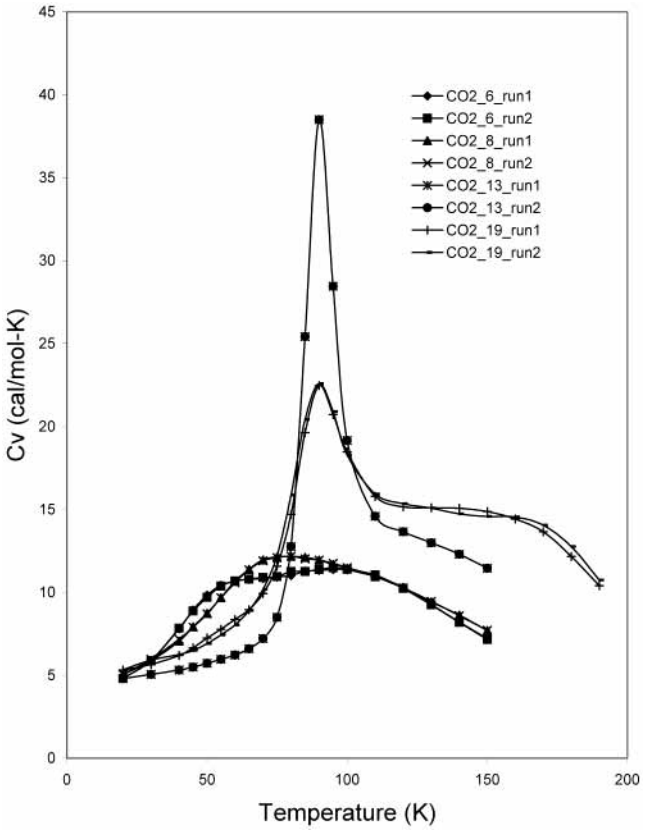

Figure 1. Heat capacity curves of the $(CO_2)_n$ clusters calculated by means of parallel tempering Monte Carlo simulations. For each cluster, run1 denotes the simulation starting from global minimum and run2 denotes the simulation starting from a random geometry.

2.c. Disconnectivity Graphs. Over the past few years much progress has been made in establishing the relationship between the topology of the potential energy surface and the difficulty of achieving equilibrium in finite temperature (or energy) simulations.[18,20,21] This requires locating the local potential energy minima and the transition states connecting the minima. In the present study, this was accomplished by carrying out eigenmode-following (EF)[8−10] searches in directions, both parallel and antiparallel to specific eigenvectors of the Hessian, for each of the minima located in the course of the optimizations. Searches were done along the eigenvector associated with the lowest 8, 15, 24, and 50 eigenvalues for $(CO_2)_6$, $(CO_2)_8$, $(CO_2)_{13}$, and $(CO_2)_{19}$, respectively. For each transition state located in this manner, subsequent searches were carried out to identify the minima connected to the transition state, allowing construction of the rearrangement pathways. These results were used to construct disconnectivity graphs,[21] which show the minima that are accessible at different energy thresholds and thus provide a convenient visual representation of the connectivity/disconnectivity of different regions of the potential energy surface.[22,23]

3. Results

The heat capacity vs temperature curves, obtained from the parallel-tempering simulations, are shown in Figure 1. For each cluster, curves from both the simulation started at the global minimum structure and that started from a randomly selected

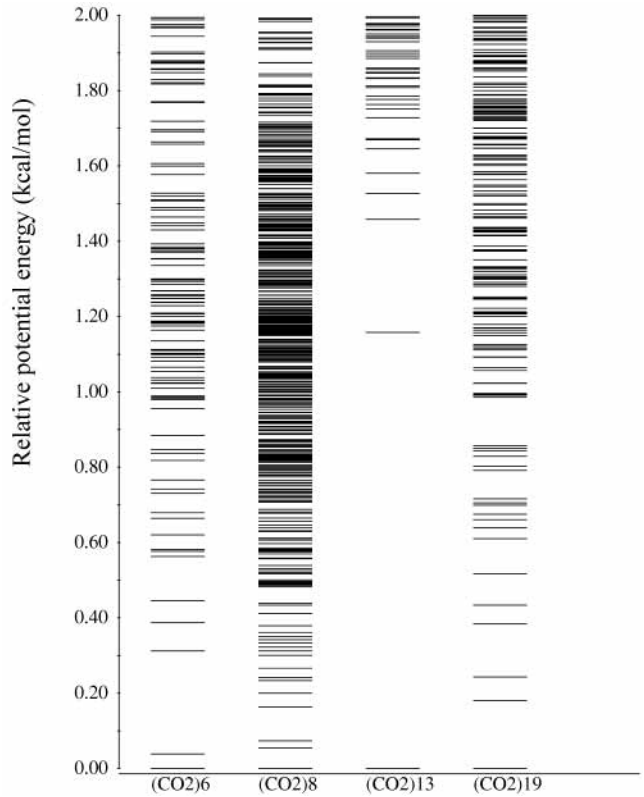

Figure 2. Energy level diagram for the $(CO_2)_n$ clusters. Each horizontal line corresponds to the energy of a local minimum as determined from quenching calculations.

structure are reported and found to be in excellent agreement, providing evidence that the calculations have achieved equilibrium. The heat capacity curves of $(CO_2)_6$ and $(CO_2)_8$ display broad, weak peaks centered near $T = 70$ K. In contrast, the heat capacity curves of $(CO_2)_{13}$ and $(CO_2)_{19}$ display pronounced, narrower peaks near $T = 90$ K. In analyzing these results, it is useful to examine the low-energy minima from the EF optimizations, the distributions of inherent structures sampled in the finite temperature simulations, and the disconnectivity graphs. The energies of the low-lying local minima of the various clusters are indicated in Figure 2. The analyses of the results for various clusters are presented below.

3.a. $(CO_2)_6$. The six lowest-energy minima of $(CO_2)_6$ obtained from the EF optimizations are shown in Figure 3. These isomers are very close in energy, being spread over only 0.57 kcal/mol. The global minimum, which can be viewed as two interacting cyclic trimers, is only 0.04 kcal/mol more stable than the second lowest-energy isomer with an octahedral-like structure, which, in turn, is only 0.28 kcal/mol stable than the next lowest-energy structure (see Figure 2).

Figure 4 reports the distributions of inherent structures of $(CO_2)_6$ sampled in the $T = 20$, 55, 80, and 100 K replicas. In the $T = 20$ K replica, only the two lowest-energy inherent structures have significant population. The populations of these two isomers gradually decrease and those of the higher energy structures gradually grow in with increasing temperature. At $T = 55$ K, which corresponds to a weak, low-temperature shoulder on the broad peak on the heat capacity curve, the six lowest-energy structures account for about 70% of the inherent structure distribution. Even at $T = 100$ K, the two lowest-energy structures together still account for about 9% of the population and the six lowest-energy structures for about 32% of the population. Although Etters et al.[2] concluded that $(CO_2)_6$ undergoes a melting transition near 70 K, in our opinion, the

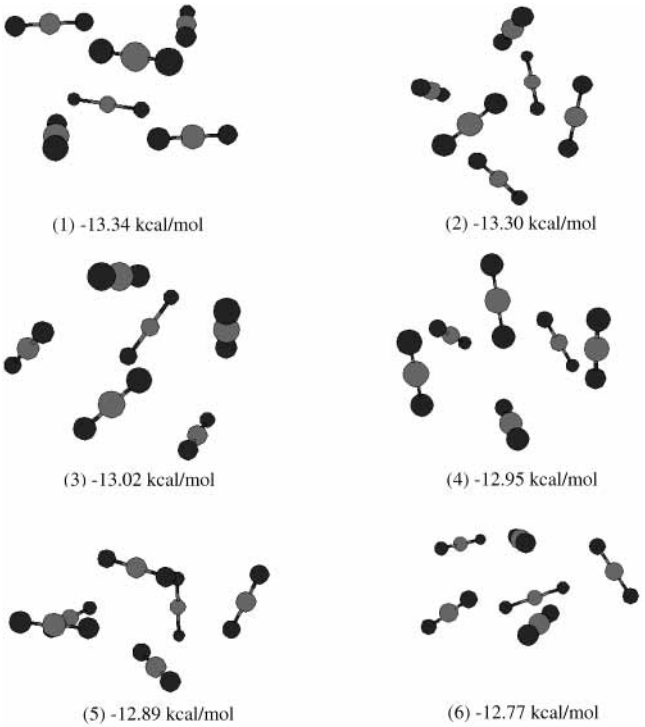

Figure 3. Structures of the six lowest-energy minima of $(CO_2)_6$ from eigenmode-following optimizations.

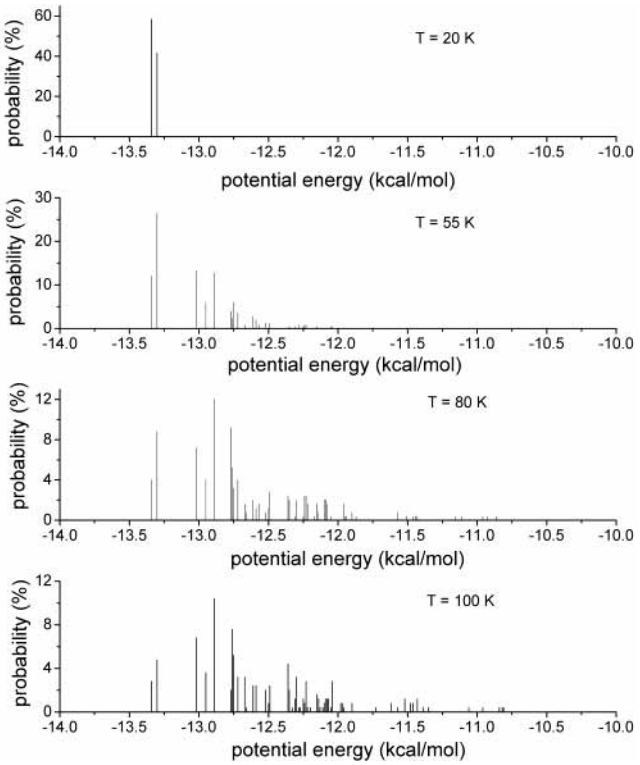

Figure 4. Distributions of local minima generated by quenching configurations from parallel tempering Monte Carlo simulations on $(CO_2)_6$.

density of states at this temperature is not sufficiently high to attribute the broad, weak peak in the heat capacity curve to a melting transition.

The disconnectivity graph for $(CO_2)_6$ is shown in Figure 5. Overall, the diagram is quite simple, and the potential energy surface can be characterized as having a single funnel. There is a barrier of about 1 kcal/mol for interconversion of the two

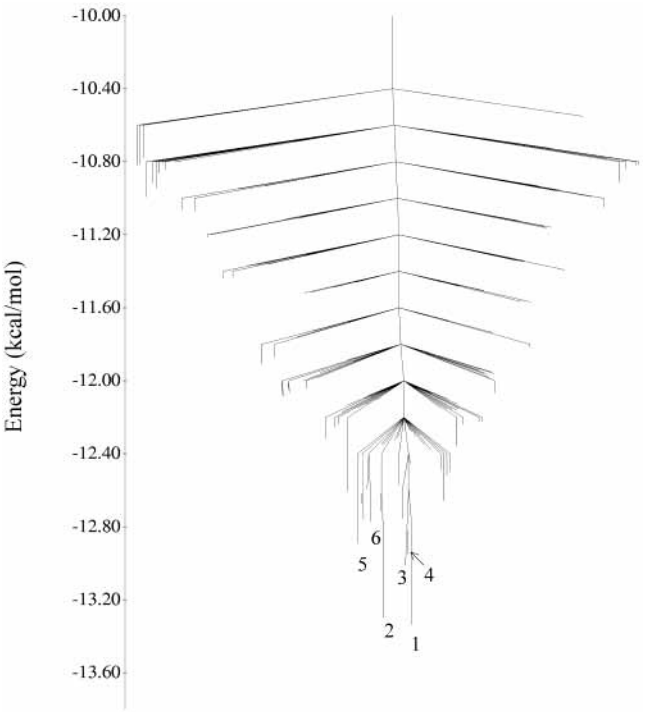

Figure 5. Disconnectivity graph for the $(CO_2)_6$ cluster. The numbers designate the low-energy structures depicted in Figure 3.

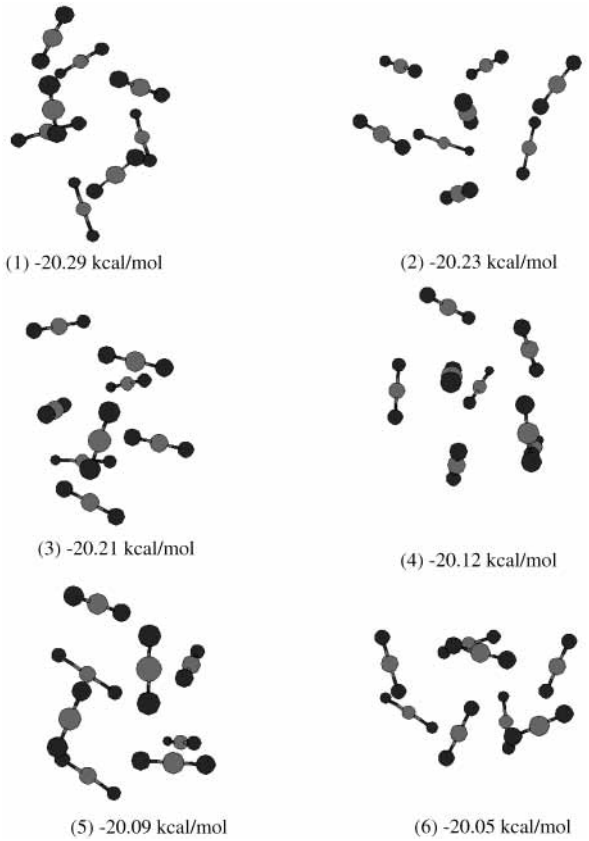

Figure 6. Structures of the six lowest-energy minima of $(CO_2)_8$ from eigenmode-following optimizations.

lowest-energy isomers. Thus it should be possible to achieve sizable populations of both these isomers in a seeded expansion.

3.b. $(CO_2)_8$. The $(CO_2)_8$ cluster possesses a very large number of low-lying potential energy minima. In fact, we have identified 158 minima within 1 kcal/mol and 490 minima within 2 kcal/mol of the global minimum. These are considerably in excess of the number of local minima found for the $(CO_2)_6$, $(CO_2)_{13}$, and $(CO_2)_{19}$ clusters in the same energy ranges.

The six lowest-energy isomers of $(CO_2)_8$, fall within an energy range of 0.24 kcal/mol and are depicted in Figure 6. The inherent structure distributions for $(CO_2)_8$ are reported in Figure 7. For the $T = 20$ K replica, the global minimum structure is most populated (~73%), with about 20% of the remaining population being associated with the second lowest-energy isomer. In the $T = 50$ K replica, the population of the two lowest-energy isomers combined has dropped to 40%, with most of the remaining population being spread over a group of isomers with inherent structure energies ranging from −20.3 to −19.8 kcal/mol. In the $T = 80$ K replica, the net population of the two lowest-energy isomers has dropped to about 7%, with the remaining population being spread over a large number of isomers.

The disconnectivity graph for $(CO_2)_8$ is shown in Figure 8. The potential energy surface of this cluster is characterized by two low-energy basins, each containing about 20 local minima. There is a barrier of about 1 kcal/mol between the lowest-energy structure in one basin to the lowest-energy structure in the other basin. Comparison of Figures 7 and 8 reveals that near $T = 70$ K the $(CO_2)_8$ cluster has an appreciable population of higher-energy structures associated with the two low-energy basins as well as of a large number of structures associated with other regions of the potential energy surface. While, the density of inherent structures is high enough to view the cluster as "liquid-like" for temperatures above about 80 K, this system does not possess a sizable energy gap between the global minimum or small group of low-energy minima and the remaining higher-lying minima (see Figure 2), and it has been argued that such an energy gap is required for a cluster to display a well-defined melting transition.[24] Due to the absence of the energy gap, the broad transition found for $(CO_2)_8$ can be viewed as "glass-like" rather than originating from a well-defined melting transition.

3.c. $(CO_2)_{13}$. The structures of the six lowest-energy isomers of the $(CO_2)_{13}$ cluster are shown in Figure 9. In agreement with ref 5, the global minimum has an icosahedral-like structure of S_6 symmetry. The global minimum is predicted to be 1.16 kcal/mol more stable than the second lowest-energy isomer, which belongs to a group of isomers with distorted icosahedral structures. This situation is analogous to that for the LJ_{13} cluster, for which the global minimum is a highly stable icosahedral structure, followed in energy by a group of distorted-icosahedral isomers, and then by non-icosahedral structures.[25]

The inherent structure distributions of $(CO_2)_{13}$ are reported in Figure 10. Only the global minimum structure has an appreciable population in the $T = 20$ K replica. Even at $T = 60$ K, it accounts for over 99% of the total population. However, at $T = 90$ K, the population of the global minimum structure has dropped to about 43%, with the remaining population being spread over a large number of higher-energy structures. At $T = 110$ K, the population of the global minimum structure has fallen to below 0.5%.

The inherent structure distributions and the large peak in the heat capacity curve of $(CO_2)_{13}$ are both indicative of a relatively sharp melting transition near 90 K. This is in agreement with Maillet et al.,[4] who concluded on the basis of molecular dynamics simulations that the $(CO_2)_{13}$ cluster melts near $T = 95$ K. The disconnectivity graph for $(CO_2)_{13}$ shown in Figure 11 displays a single-funnel topology similar to that found for LJ_{13}.[21]

3.d. $(CO_2)_{19}$. The geometries of the six lowest-energy isomers of $(CO_2)_{19}$ are shown in Figure 12. All of these may be viewed

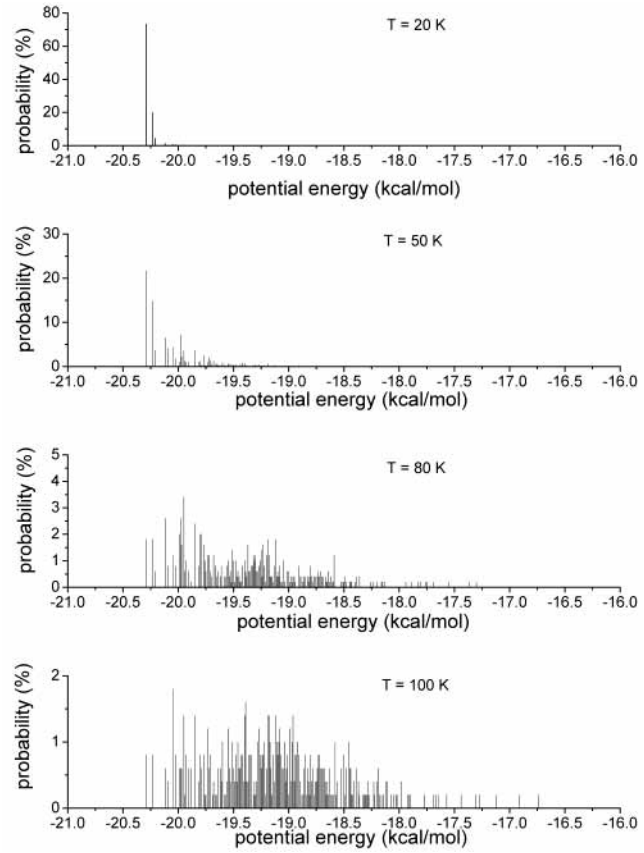

Figure 7. Distributions of local minima generated by quenching configurations from parallel tempering Monte Carlo simulations on $(CO_2)_8$.

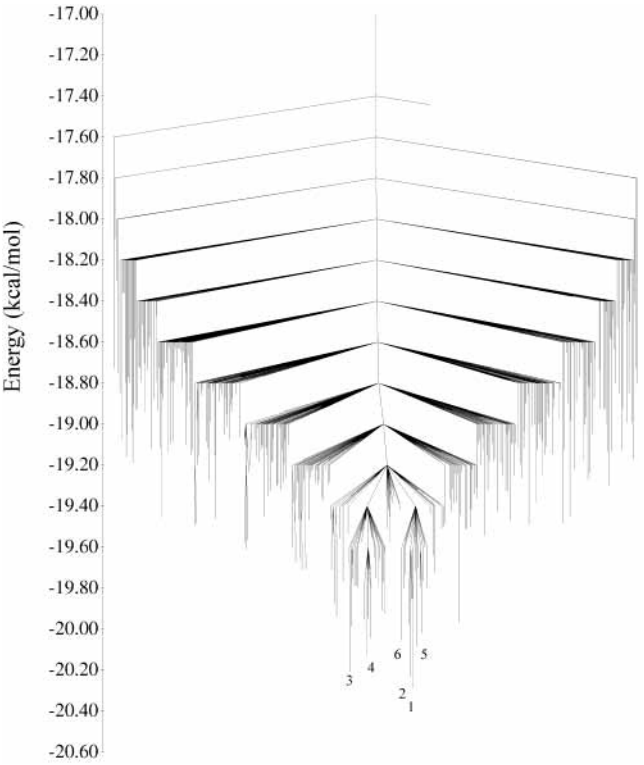

Figure 8. Disconnectivity graph for the $(CO_2)_8$ cluster. The numbers designate the low-energy structures depicted in Figure 6.

as icosahedral-like with an approximately icosahedral $(CO_2)_{13}$ core and with the remaining six molecules forming a surface layer. These six isomers are close in energy, being spread over

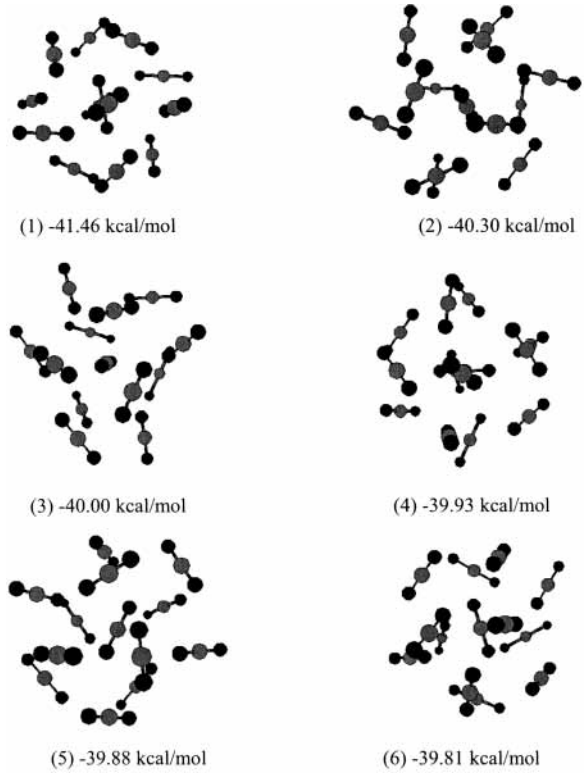

Figure 9. Structures of the six lowest-energy minima of $(CO_2)_{13}$ from eigenmode-following optimizations.

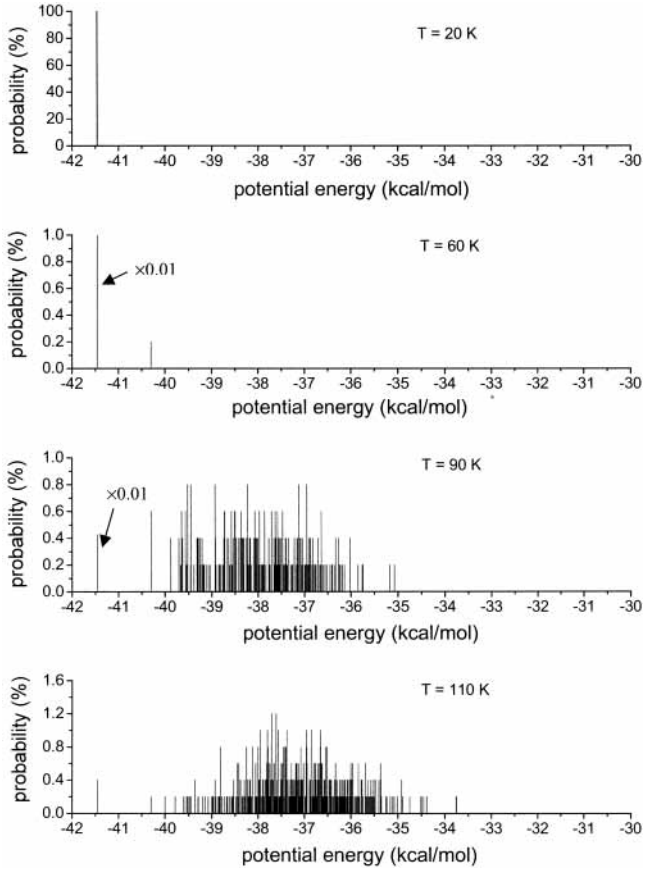

Figure 10. Distributions of local minima generated by quenching configurations from parallel tempering Monte Carlo simulations on $(CO_2)_{13}$.

only 0.5 kcal/mol. The inherent structure distributions are plotted in Figure 13. For the T = 20 K replica, about 87% of the

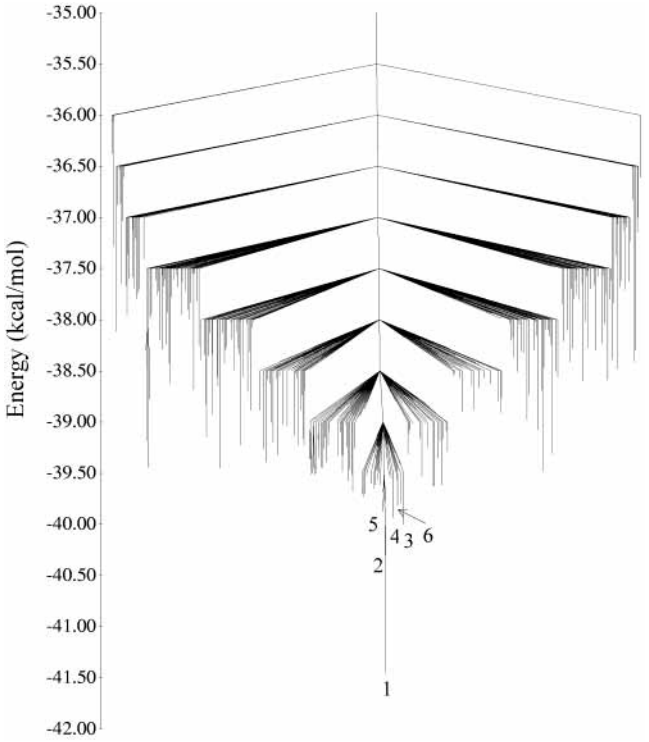

Figure 11. Disconnectivity graph for the $(CO_2)_{13}$ cluster. The numbers designate the low-energy structures depicted in Figure 9.

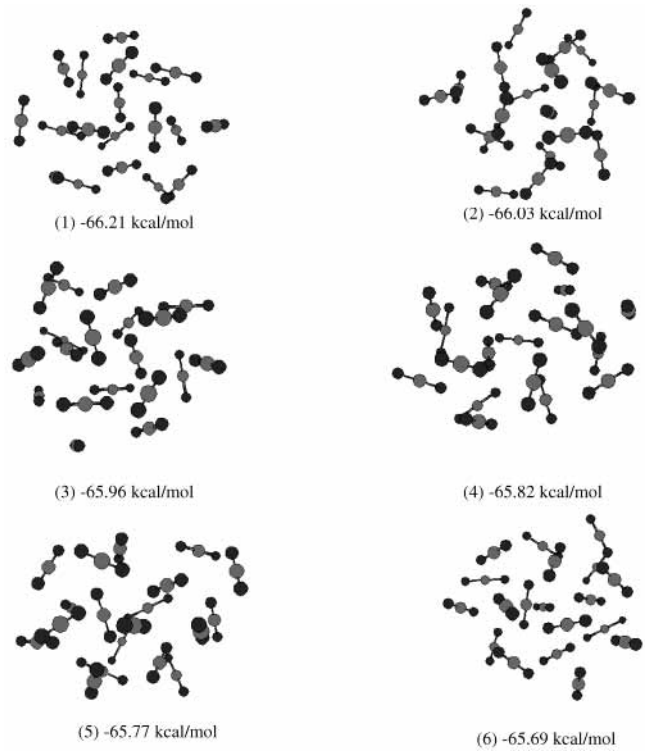

Figure 12. Structures of the six lowest-energy minima of $(CO_2)_{19}$ from eigenmode-following optimizations.

population is associated with the global minimum, with the remaining population being due to the next two-lowest energy isomers. At $T = 50$ K, these three isomers still dominate, but now isomer **2**, is most populated at 38%. At $T = 80$ K, somewhat below the temperature of the maximum in the large peak in the heat capacity curve, the net population of the three lowest-energy isomers has fallen to about 8%, with the remaining population being distributed over a large number of

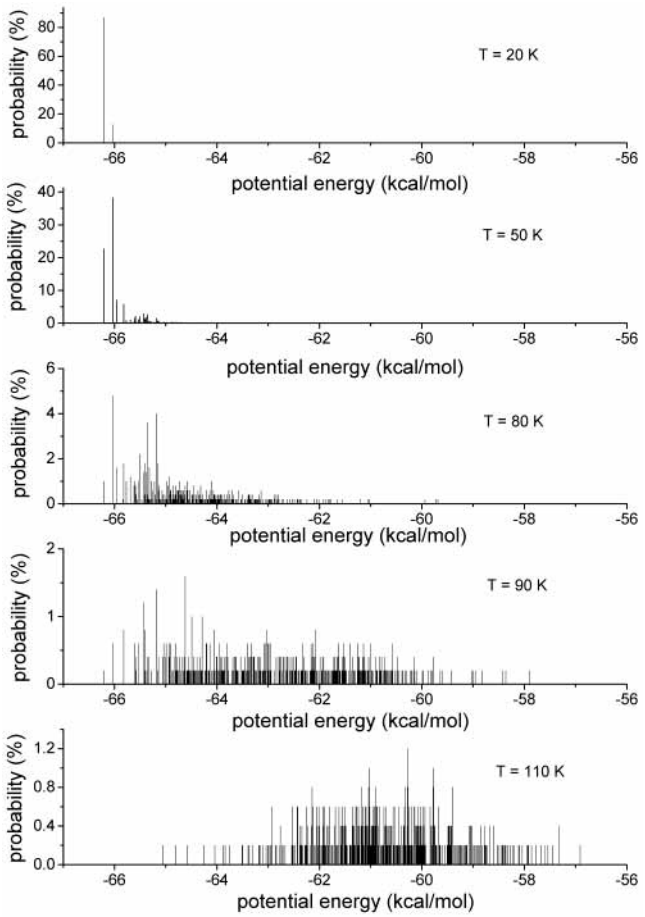

Figure 13. Distributions of local minima generated by quenching configurations from parallel tempering Monte Carlo simulations on $(CO_2)_{19}$.

higher-lying isomers. At $T = 100$ K, there is no significant population of the six lowest-energy isomers. The trends in the inherent structure distributions provide strong evidence that the large peak near 90 K in the heat capacity curve of $(CO_2)_{19}$ is due to a melting-like transition. This is consistent with the conclusion of Maillet et al.,[5] who reported, on the basis of molecular dynamics simulations, that $(CO_2)_{19}$ melts near $T = 95$ K.

The heat capacity curve for $(CO_2)_{19}$ also displays a weak shoulder near $T = 50$ K. This is due to a "solid"-to-"solid" transition between isomer **1** and isomers **2** and **3**. This interpretation is supported by the disconnectivity graph of $(CO_2)_{19}$ shown in Figure 14, which reveals that each of the three low-energy isomers is associated with a different basin. The barriers to go from the lowest-energy isomer to the basins containing isomers **2** and **3** are over 3 kcal/mol.

4. Conclusions

In this paper the finite temperature behavior of the $(CO_2)_n$, $n = 6$, 8, 13, and 19, clusters has been investigated by means of parallel-tempering Monte Carlo simulations. The results have been analyzed in terms of inherent structure distributions and disconnectivity graphs. The question of when to characterize a structural transformation in a small cluster as a melting transition has been the subject of much discussion in the literature.[24,26−27] For the present purposes, in labeling a transition as "melting", we required that the transition display a pronounced, sharp peak in the heat capacity curve and that, over the range of temperatures corresponding to the rapid variation in the heat capacity,

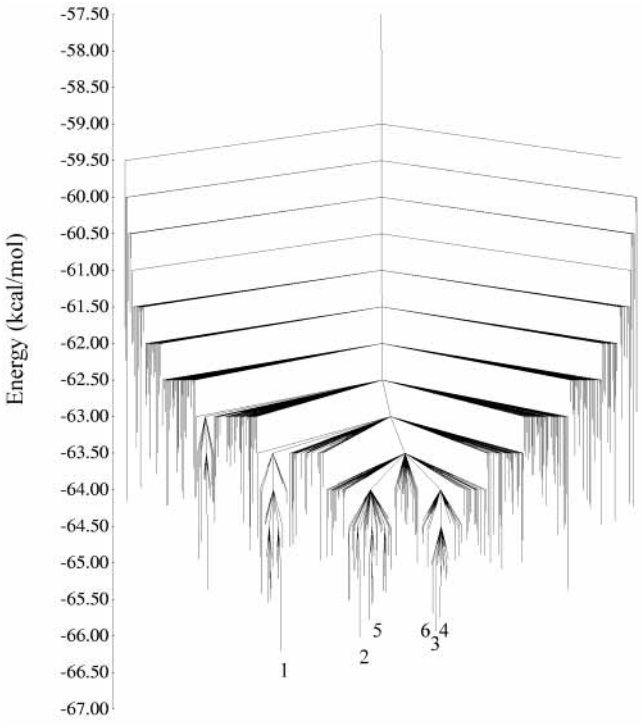

Figure 14. Disconnectivity graph for the $(CO_2)_{19}$ cluster. The numbers designate the low-energy structures depicted in Figure 12.

the system evolves from having an appreciable population in a small number of low-energy structures to a having the population spread over a large number of higher-lying structures. We have further required that there be a sizable energy gap between the structures important on the low-temperature side of the heat capacity peak and those important on the high-temperature side. On the basis of these criteria it is concluded that the sharp peaks near $T = 90$ K in the heat capacity curves of $(CO_2)_{13}$ and $(CO_2)_{19}$ are due to melting-type transitions whereas the broad peak in heat capacity curve of $(CO_2)_6$ should not be taken as indicative of melting. Although the broad peak in the heat capacity curve of $(CO_2)_8$ is similar in appearance to that of $(CO_2)_6$, these two clusters differ appreciably in the topologies of their potential energy surface as reflected in their disconnectivity graphs. However, due to the absence of a sizable energy gap between a group of low-energy structures and the higher-energy structures populated near $T = 70$ K, we conclude that $(CO_2)_8$ also does not undergo a well-defined melting transition. The broad shoulder near T = 50 K in the heat capacity curve of $(CO_2)_{19}$ is attributed to a "solid−solid-like" transition.

Acknowledgment. This research was carried out with a support from a grant from NSF. The calculations were carried out on the IBM RS6000 workstation cluster in Center for Molecular and Materials Simulations (CMMS) at the University of Pittsburgh. The computers in CMMS were funded by grants from NSF and IBM. We thank Drs. Mark Miller and David Wales for access to their program to construct the disconnectivity tree graphs, and Arnold Tharrington for assistance in using his parallel tempering Monte Carlo code.

References and Notes

(1) Stone, A. J. *The Theory of Intermolecular Forces*; Calrendon Press: Oxford, 1996.
(2) Etters, R. D.; Flurchick, K.; Pan, R. P. *J. Chem. Phys.* **1981**, *75*, 929.
(3) Torchet, G.; deFeraudy, M. F.; Boutin, A.; Fuchs, A. H. *J. Chem. Phys.* **1996**, *105*, 3671−3678.
(4) Maillet, J. B.; Boutin, A.; Buttefey, S.; Calvo, F.; Fuchs, A. H. *J. Chem. Phys.* **1998**, *109*, 329−337.
(5) Maillet, J. B.; Boutin, A.; Fuchs, A. H. *J. Chem. Phys.* **1999**, *111*, 2095−2102.
(6) Van de Waal, B. W. *J. Chem. Phys.* **1987**, *86*, 5660.
(7) Neirotti, J. P.; Calvo, F.; Freeman, D. L.; Doll, J. D. *J. Chem. Phys.* **2000**, *112*, 10340−10349.
(8) Cerjan, C. J.; Miller, W. H. *J. Chem. Phys.* **1981**, *75*, 2800.
(9) Tsai, C. J.; Jordan, K. D. *J. Phys. Chem.* **1993**, *97*, 11227−11237.
(10) Miller, M. A.; Doye, J. P. K.; Wales, D. J. *J. Chem. Phys.* **1999**, *110*, 328−334.
(11) Murthy, C. S.; O'Shea, S. F.; McDonald, I. R. *Mol. Phys.* **1983**, *50*, 531.
(12) Weida, M. J.; Sperhac, J. M.; Nesbitt, D. J. *J. Chem. Phys.* **1995**, *103*, 7685−7699.
(13) Jordan, K. D. Unpublished work.
(14) Bukowski, R.; Sadlej, J.; Jeziorski, B.; Jankowski, P.; Szalewicz, K. *J. Chem. Phys.* **1999**, *110*, 3785−3803.
(15) Jorgensen, W. L.; Chandrasekhar, J.; Madura, J. D. *J. Chem. Phys.* **1983**, *79*, 926.
(16) Geyer, C. J.; Thompson, E. A. *J. Am. Stat. Assoc.* **1995**, *90*, 909−920.
(17) Tesi, M. C.; vanRensburg, E. J. J.; Orlandini, E.; Whittington, S. G. *J. Stat. Phys.* **1996**, *82*, 155−181.
(18) Munro, L. J.; Tharrington, A.; Jordan, K. D. *Comput. Phys. Commun.* **2002**, *145*, 1−23.
(19) Popelier, P. L. A.; Stone, A. J. *Mol. Phys.* **1994**, *82*, 411−425.
(20) Pedulla, J. M.; Jordan, K. D. *Chem. Phys.* **1998**, *239*, 593−601.
(21) Doye, J. P. K.; Miller, M. A.; Wales, D. J. *J. Chem. Phys.* **1999**, *110*, 6896−6906.
(22) Doye, J. P. K.; Miller, M. A.; Wales, D. J. *J. Chem. Phys.* **1999**, *111*, 8417−8428.
(23) Becker, O. M.; Karplus, M. *J. Chem. Phys.* **1997**, *106*, 1495−1517.
(24) Beck, T. L.; Berry, R. S. *J. Chem. Phys.* **1988**, *88*, 3910.
(25) Deaven, D. M.; Tit, N.; Morris, J. R.; Ho, K. M. *Chem. Phys. Lett.* **1996**, *256*, 195−200.
(26) Labastie, P.; Whetten, R. L. *Phys. Rev. Lett.* **1990,** *65*, 1567−1570.
(27) Lynden-Bell, R. M.; Wales, D. J. *J. Chem. Phys.* **1994,** *101*, 1460−1476.